

# Nanomaterial Deposits Formed by DC Plasma Spraying of Liquid Feedstocks

Jeganathan Karthikeyan, Christopher C. Berndt,\* Sri Reddy, Jenn-Yue Wang, Alexander H. King,\* and Herbert Herman\*

The Thermal Spray Laboratory, Department of Materials Science and Engineering, State University of New York at Stony Brook, Stony Brook, New York 11794-2275

**An experimental system consisting of an axial feed plasma gun, a variable-rate liquid delivery system, a liquid atomizer-feeder, and a substrate movement and control system was designed and assembled for preparing nanograined ceramic deposits. Sprayed deposits were produced with different spray and sol feed parameters and investigated in both the as-sprayed and heat-treated conditions. As-sprayed deposits were predominately hydroxide phases and were strongly adherent to the substrates. Postspray heat treatment at 873 K led to conversion of the alumina and zirconia deposits to  $\gamma$ -alumina and tetragonal zirconia phases, respectively. Subsequent heat treatment at 1273 K resulted in densification of the deposits and formation of high-temperature phases. A small increase in the grain size was observed with heat treatment, but the specimens still retained nanosized grains.**

## I. Introduction

CERTAIN physical and mechanical properties of materials exhibit remarkable improvements as their grain size is reduced from the micrometer to the nanometer range.<sup>1-5</sup> Attractive features include the ability to sinter and densify at low temperatures, hardness, ductility, and unique magnetic, optical, and dielectric properties. These features are expected to find applications in many advanced industries. Hence, during the last 10 to 15 years, many laboratories in the United States,<sup>1</sup> Japan,<sup>6</sup> and Germany<sup>7</sup> have investigated nanoscience and technology. Various techniques such as sol-gel,<sup>8</sup> vapor deposition,<sup>9</sup> laser ablation,<sup>10</sup> mechanical milling,<sup>2</sup> flame pyrolysis,<sup>11</sup> and rf and microwave plasma synthesis<sup>12,13</sup> have been developed and/or modified to synthesize nanomaterials. A critical look at the status of nanotechnology<sup>1-13</sup> shows that most of the workers have concentrated on the synthesis of various nanomaterials, but little work has been reported on consolidation of these nanoparticles. Studies carried out to consolidate nanomaterials have shown that these powders have inherent metastability and a strong tendency for rapid grain growth, and that the conventional powder metallurgy techniques such as sintering and hot pressing can lead to difficulties in achieving full consolidation while preserving the nanometer size of the starting materials.<sup>14,15</sup> Coating technology which combines the synthesis and consolidation processes into a single operation can be advantageously used to avoid some of the problems encountered during conventional consolidation procedures. Moreover,

many engineering applications such as wear resistance coatings or thermal barriers require enhanced properties at the surface only. This, coupled with the high cost of manufacturing and processing of nanomaterials, indicates that nanomaterial deposits will find engineering applications in many industries before the monoliths can be industrially employed.<sup>8</sup>

The plasma spray process<sup>16</sup> is one of the widely used techniques for producing overlay coatings for various industrial applications. This process uses a high-temperature, high-velocity plasma jet to melt and spray 10-100  $\mu\text{m}$  sized feedstock to form an overlay coating. In general, the plasma spray process uses a solid feedstock and produces fine-grained (0.5 to 5.0  $\mu\text{m}$ ) deposits. When finer-sized particles are used as the feedstock material, coatings with thinner lamella and improved properties are obtained.<sup>17</sup> Hence, if the solid particles are replaced by atomized liquid droplets, further reduction in the grain size can occur and lead to the formation of nanodeposits having superior properties. However, plasma spray processing of liquid precursors has not been reported in the open literature. This article presents a study carried out to produce nanomaterial deposits by a technique, termed as plasma spraying of liquid precursors (PSLP).

As a technique for producing nanodeposits, the PSLP has many advantages such as simple processing, versatility to produce almost any deposit over any substrate, capability to produce thick film deposits, high deposition rate ( $>5 \mu\text{m}/\text{min}$ ), and flexibility to produce complex composite deposits using liquid mixtures or multiple feeders. The PSLP is an aerosol process, and it has some advantages over the conventional plasma spray process. In conventional plasma spraying, since deposits are produced with 10-100  $\mu\text{m}$  sized particles, they have variation in chemical compositions over distances of tens of micrometers.<sup>18</sup> In the PSLP process, each droplet of the liquid feedstock contains the stoichiometric composition of the desired final product, and hence deposits with compositional homogeneity are produced.<sup>19</sup>

## II. Experimental System

The PSLP system consists of a liquid feeder, a liquid atomizer-injector, an atmospheric plasma spray system, and a substrate holder-manipulator (Fig. 1(a)). The liquid feeder delivers measured quantities of the feedstock to the atomizer-injector, which produces atomized droplets of the feedstock and injects them into the high-pressure plume of the plasma jet. An axial feed plasma spray<sup>20</sup> torch (electromagnetically coalesced plasma spray gun, Flame-Spray Industries, NY), with a modified powder injection port to incorporate the injector, is used to produce the high-temperature plasma flame. As the droplets enter the plasma plume, heat and momentum transfer from the plasma into the droplet lead to the evaporation of the solvent, condensation of the precursor, and plasma chemical reactions, resulting in the formation of a dense and coherent deposit.

The liquid feedstock feeder, shown in Fig. 1(b), is a pressurized chamber incorporating a stirring mechanism. The de-

L. C. Klein--contributing editor

Manuscript No. 192046. Received February 5, 1996; approved November 15, 1996. Supported by the U.S. National Science Foundation under Grant No. CTS-9312896.

\*Member, American Ceramic Society.

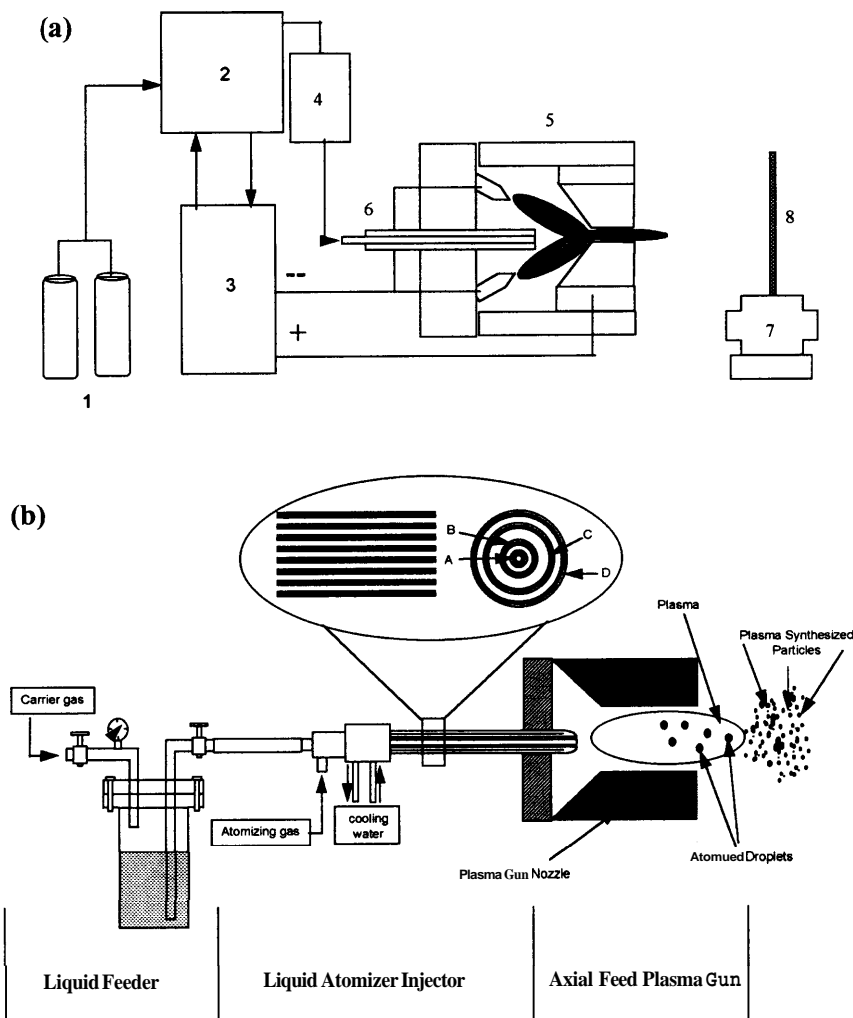


**Fig. 1.** (a) Schematic of the plasma spray processing system: (1) gas supply, (2) control console, (3) power supply, (4) liquid feeder, (5) EMC plasma gun, (6) liquid atomizer injector, (7) substrate manipulator, and (8) substrate. (b) Schematic of the liquid atomizer-injector.

livery rate of the liquid can be varied in the range of 26.2 to 51.0 mL/min by varying the gas pressure from 0.1 to 0.3 MPa. Solenoid valves, pressure regulators, and gauges, installed at the pressure vessel and at different locations along the flow paths, are used to measure and control the pressures and flow rates of both fluids.

The liquid atomizer-injector works on the two-fluid atomization principle<sup>21</sup> with nitrogen as the atomizing gas. As can be seen in Fig. 1(b), this injector has four thin-walled coaxial tubes. Liquid is injected into the innermost (tube A) tube (1.525 mm diameter and 225 mm long). An atomizing gas, flowing through the coaxial outer (tube B) tube (2.350 mm diameter and 212 mm long), atomizes the liquid and injects it into the plasma jet. Injector cooling water flows in and out of the third (tube C) and fourth (tube D) tubes, respectively. The outermost (tube D) tube (6.250 mm diameter and 200 mm) contains the adapter for mounting the injector onto the plasma gun.

The axial-feed gun used in this work consists of four pilot plasma torches which operate in a conventional manner. The plasma flame exiting from each of these torches converges on a point located at the inlet of a main anode nozzle assembly (see Fig. 1(a)). The magnetic field surrounding each of the pilot plasmas electromagnetically coalesces them into a central plasma. Simultaneously, an electric current is established between the pilot plasmas and the main anode nozzle. The feedstock injector (liquid atomizer), incorporated along the axis of the gun, inserts the feedstock into the core of the plasma.

### III. Experiments

#### (1) Materials and Spray Feedstocks

Aluminum isopropoxide and 16 wt% zirconium acetate solution in acetic acid were used as metalorganic precursors. Commercially available alumina sol (Dispal 23N4-20, Vista Chemical Co., Houston, TX) was used to prepare the high-concentration alumina sol. Liquid feedstocks for spray operation were prepared by dissolving the precursors in distilled water. Inconel and mild steel coupons of dimensions 50 mm x 15 mm x 4 mm were used as substrates, and alumina grit (10 mesh) was used to grit blast the substrates prior to spray coating.

One percent molar concentration alumina sol was prepared as follows. A quantity of 300 g of deionized and distilled water was heated to 353 K and then 34.01 g of aluminum isopropoxide was slowly added, stirring vigorously. The solution was then stirred for 20 min, and 1.5 mL of concentrated nitric acid added such that the slurry had a molar ratio of acid/hydroxide of 0.154. The slurry temperature was maintained at 353 K for another 6 h for the peptization to be completed and to produce a clear sol. High-concentration alumina sol (10%) was prepared by diluting 100 mL of the Vista sol with 100 mL of distilled water. Similarly, 1000 g of zirconium acetate in dilute acetic acid was further diluted with 520 mL of distilled water to obtain 2 wt% zirconia feed liquid.

## (2) Characterization of the Liquid Atomizer Injector

The laser scattering technique,<sup>22</sup> which uses the intensity of the scattered laser light to record the size distribution of the scattering media, was used to study the performance of the liquid atomizer-injector. The feed rate of the liquid and the pressure of the atomizing gas were varied in the ranges of 15.0 to 50.0 cm<sup>3</sup>/min and 2.0 to 5.0 bar, respectively, and their effect on the droplet size distribution of the atomized fluid was recorded. These experiments were carried out in atmospheric air using water and compressed air as the atomized and atomizing fluids, respectively.

## (3) Deposit Preparation and Heat Treatment

Initial efforts to produce deposits by injecting a liquid jet, instead of an aerosol, into the plasma jet resulted in severe erosion of the copper nozzle and produced deposits with copper and copper oxide contamination. Hence all subsequent deposits were produced with aerosol feeding only. A series of spray experiments were carried out to establish the optimum spray parameter values which yield quality deposits at a reasonable deposition efficiency. Optimized spray parameter values for spraying both alumina and zirconia sols, established from the results of these experiments, are presented in Table I.

Sprayed specimens were heat-treated at low (873 K) and high (1273 K) temperatures for 1.0 h in air with heating and cooling rates of 5 K/min. As-sprayed and heat-treated specimens were subjected to investigations to determine the variation in phase composition and microstructure of the specimen, and to establish the chemical reaction routes.

## (4) Specimen Characterization

Microstructural features of the specimens were studied using optical and scanning electron microscopes (Model JSM 5300, Joel, Tokyo, Japan). X-ray diffraction (Model PW 1729, Philips) was used to establish the phase composition of the specimen. XRD was also used to estimate the deposit grain size as follows.<sup>23-25</sup> The diffraction pattern of the specimen was recorded at a speed of 0.01°/s using CuK $\alpha$  radiation with a nickel filter, and the full widths at half-maximum (FWHM) of the diffraction peaks were measured. Contributions due to K $\alpha$ <sub>1</sub> and K $\alpha$ <sub>2</sub> were deconvoluted, and only the K $\alpha$ <sub>1</sub> peak widths were used for calculation. XRD of a standard silica specimen was used to measure instrument broadening, and Ziegler's method was used to remove the instrument broadening for obtaining the true crystal broadening.<sup>24</sup> Using the Scherrer relationship for size effect and Cauchy's correction for stress effects, the following relationship is obtained:

$$\beta \cos \theta = K\lambda/D + 4\Delta d/(d \sin \theta) \quad (1)$$

where D is the size of the crystallite, K is the shape constant (close to unity),  $\lambda$  is the wavelength of the radiation,  $\beta$  is the corrected true FWHM of the diffraction peak,  $\theta$  is the diffraction angle, and Ad and d are the average lattice strain and dimension, respectively.

**Table I. Parameters for Spraying Alumina and Zirconia Sols**

Parameter	Alumina	Zirconia
Power (kW)	25.2 (low) 41.0 (high)	29.0 (low) 41.0 (high)
Plasma gas 1 (Ar-SLPM)	55.0	38.0
Plasma gas 2 (Ar-SLPM)	0.0	12.0
Stand-off distance (mm)	80.0	100.0
Atomizer gas pressure (kg/cm <sup>2</sup> )	3.0	4.0
Feedstock concentration (%)	1.0 (low) 10.0 (high)	2.0 (low) 5.0 (high)
Feedstock flow rate (mL/min)	30.0 (low) 50.0 (high)	30.0

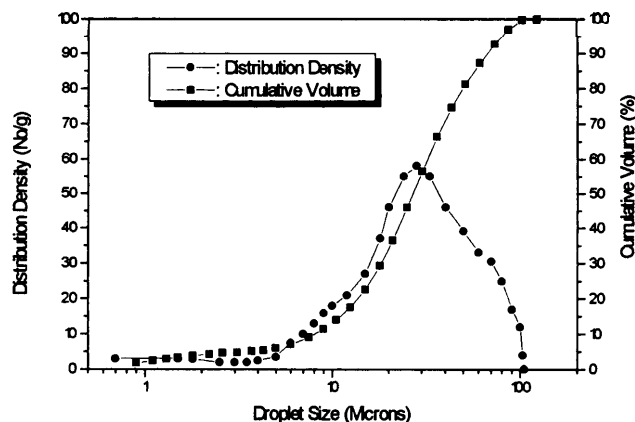


**Fig. 2.** Droplet size distribution of liquid atomizer-injector produced aerosol.

The parameter  $\beta \cos \theta$  was plotted versus  $\sin \theta$ , and as shown by Eq. (1), a straight line is obtained with the intercept given by the crystal size and the slope revealing the stress effect. However, it should be noted that the experimental technique, correction procedure, and deconvolution process strongly effect<sup>23-25</sup> the estimated grain size, and hence the XRD estimated grain size should be treated only as an estimate.

Typical deposits were removed from the substrate, ground, mounted onto carbon-coated copper TEM grids, ion beam thinned, and then investigated using TEM (Model CM 12, Philips). However, the specimens were found to be unstable in the TEM specimen preparation procedure and only qualitative results could be obtained.

## IV. Results

### (1) Atomizer

Typical results of the laser scattering studies (Fig. 2) show that the atomizer has produced an aerosol with a wide range of droplet sizes, varying from 1.0 to 100  $\mu$ m with mode and median values of 29 and 27  $\mu$ m, respectively. Variation of the atomizer parameters such as atomizing gas pressure and the liquid flow rate resulted in small variations in the size distribution, but the size range and median values did not show large variations.

### (2) Alumina

Typical SEM images of as-sprayed specimens are shown in Fig. 3. The deposit presents a dense and coherent microstruc-

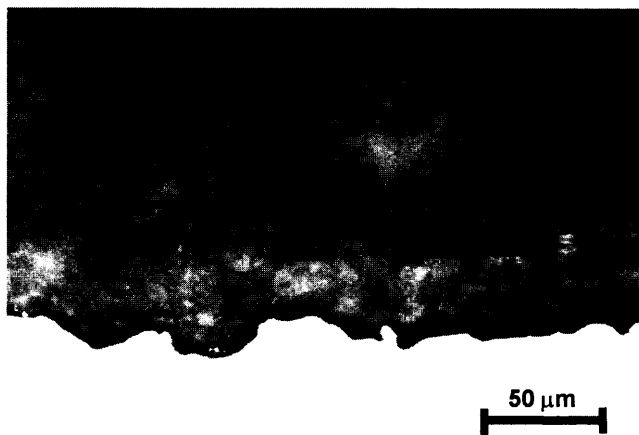


**Fig. 3.** SEM image of a typical alumina specimen.

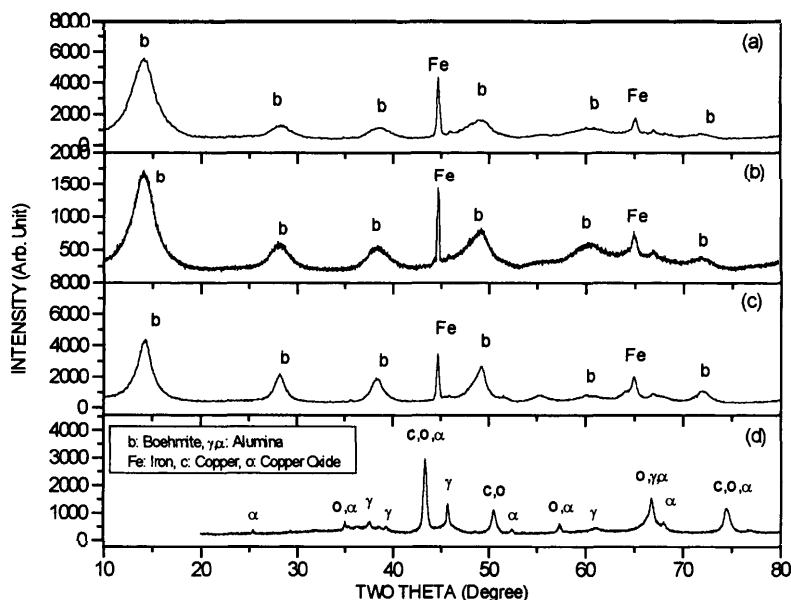


Fig. 4. XRD of as-sprayed alumina specimens: (a) low concentration and low feed rate; (b) low concentration and high feed rate; (c) high concentration and low feed rate; (d) liquid jet feed.

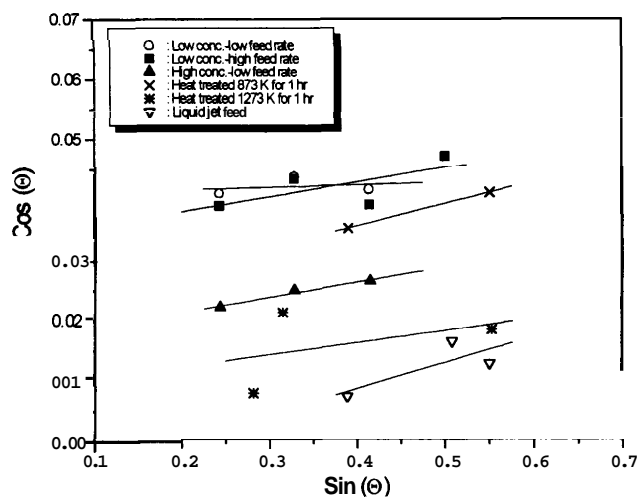


Fig. 5. Scherrer plots of alumina specimens.

ture, but does not possess the characteristic lamellar structure of a thermal spray deposit. XRD of typical deposits prepared under various processing conditions (Fig. 4) indicates that the deposit consisted of pseudo-boehmite as the dominant phase. The deposit XRD also contains the diffraction peaks of the substrate material, indicating that the deposit is discontinuous. The diffraction peaks of the deposits are all broad, showing that the deposits produced with liquid feedstocks have ultra-fine-

grained structures. The XRD of the liquid-jet-produced deposit shows copper (from the plasma gun nozzle) and copper oxide as the major phases. The XRD also shows that, in contrast to the aerosol feeding, liquid jet feeding resulted in the transformation of the AlOOH phase into  $\gamma$ - and  $\alpha$ -alumina phases.

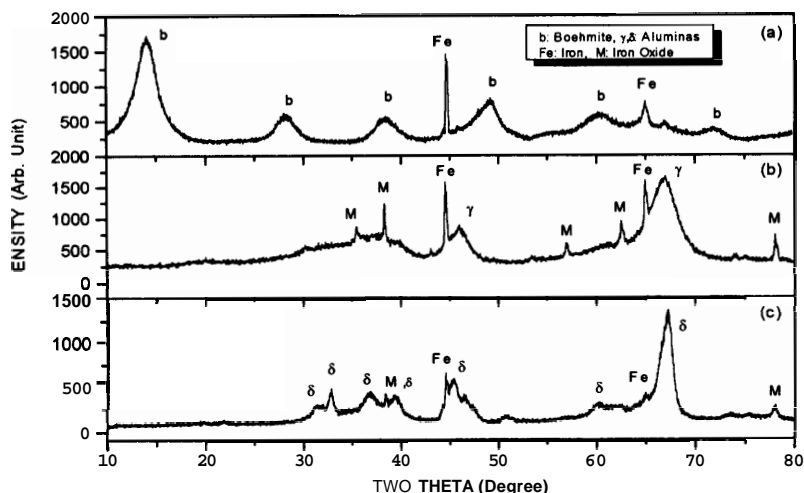
Figure 5 presents the results of the Scherrer-Cauchy analysis (Eq. (1)) of typical specimens, and the grain sizes calculated from these figures are presented in Table II. However, it should be noted that the specimen XRDs contained overlapping peak patterns of the deposit and substrate materials, and correction and deconvolution processes of these XRDs have led to errors in the measurement of the FWHM values. This error was particularly large in the case of liquid-jet-fed deposits that contained copper, copper oxide,  $\alpha$ -alumina, and  $\gamma$ -alumina, and the heat-treated specimens that contained a mixture of  $\gamma$ - and  $\alpha$ -aluminas. This error is reflected in the large scatter of the data points in Fig. 5. Hence, as noted in Section III(4), the XRD estimated grain sizes, given in Table II, should be treated as estimates only.

Table II shows that increasing the concentration of the sol leads to perceptible grain coarsening of the deposit from 5 to 10 nm. An increase in the sol feed rate results in a small increase (from 4 to 5 nm) in grain size, but the deposits still retain their fine grain structure. When the mode of sol injection is changed from atomized droplets to a liquid jet, a fourfold increase in the average grain size is observed.

The effect of heat treatment is presented in Fig. 6. The low-temperature heat treatment has changed the phase composition of the deposit from pseudo-boehmite into  $\gamma$ -alumina. Oxidation has led to the formation of magnetite ( $\text{Fe}_3\text{O}_4$ ) on the substrate surface. Heat-treating the specimen at 1273 K transformed the material into  $\alpha$ -alumina. The Scherrer analysis (Table II)

Table II. Scherrer-Cauchy Grain Size of Alumina Specimens

Specimen	Feedstock			Heat treatment	Phase	Grain size (nm)
	Feed mode	Concn (%)	Feed rate (mL/min)			
1	Atomized	1.0	30	As-spray	AlOOH	4
2	Atomized	1.0	30	As-spray	AlOOH	5
3	Atomized	10.0	30	As-spray	AlOOH	10
4	Liquid jet	1.0	30	As-spray	$\gamma$ -Alumina	21
5	Atomized	1.0	30	873 K, 1 h	$\gamma$ -Alumina	7
6	Atomized	1.0	30	1273 K, 1 h	$\alpha$ -Alumina	19



**Fig. 6.** Variation of XRD of alumina specimen with heat treatment: (a) as-sprayed, (b) heat-treated at 873 K for 1.0 h, and (c) heat-treated at 1273 K for 1.0 h.

showed that the low-temperature heat treatment resulted in a grain size increase from 4 to 7 nm, and high-temperature heat treatment resulted in grain coarsening to about 19 nm.

### (3) Zirconia

Microstructural investigations indicated that zirconia deposits also show a dense, coherent, and thermally unstable microstructure, but do not show the characteristic lamellar structure of a plasma-sprayed coating. Figure 7 presents the microstructures of typical specimens. The low-temperature heat treatment fragmented the deposit and produced a globular structure with many pores, voids, vertical cracks, and horizontal delaminations along the substrate–deposit interface. High-temperature (1273 K) heat treatment removed most of the vertical cracks and led to densification of the deposit.

X-ray studies (Fig. 8) showed that the as-sprayed deposits are predominantly amorphous zirconium hydroxide with a small amount of tetragonal (*t*) zirconia as the minor phase. These diffraction patterns also contain the diffraction peaks of the substrate material indicating that the deposits are discontinuous. Variations of the process parameters, such as the feedstock concentration and power level, had no marked effects on the sprayed deposits. Heat-treating the specimen at 873 K for 1 h transformed the material from amorphous  $Zr(OH)_4$  phase to a crystallized zirconia phase. Deconvolution of the XRD showed that the material was tetragonal zirconia, which could be identified by the presence of a complete tetragonal peak pattern and the absence of corresponding cubic peaks. For instance, as the inset in Fig. 8(b) shows, the XRD contains both tetragonal peaks (004) with  $I/I_0$  of 4 at a *d* value of 1.312 Å and (400) with  $I/I_0$  of 8 at 1.281 Å, but does not contain the cubic (400) peak at a *d* value of 1.270 Å ( $I/I_0$  of 5). Scherrer analysis showed that these specimens had ~7 nm grain size.

High-temperature (1273 K) heat treatment resulted in the conversion of most of the tetragonal zirconia grains into monoclinic zirconia, and the specimen phase structure changed to predominantly monoclinic zirconia with tetragonal zirconia as the minor phase. The Scherrer analysis indicated that the crystallite size of the monoclinic zirconia (68 nm) was about an order of magnitude larger than that of tetragonal zirconia (8 nm).

The TEM specimen preparation procedure, in particular the ion beam thinning of the specimen, led to reactions and phase transformations in the specimen, often damaging the specimen itself. A bright-field image of a typical specimen is presented in Fig. 9. The specimen is electron opaque in most regions, but, at the edges, individual particles of size 50 to 150 nm (shown by arrows) can be seen which reveal the nanosized grain/particle structure of the specimen.

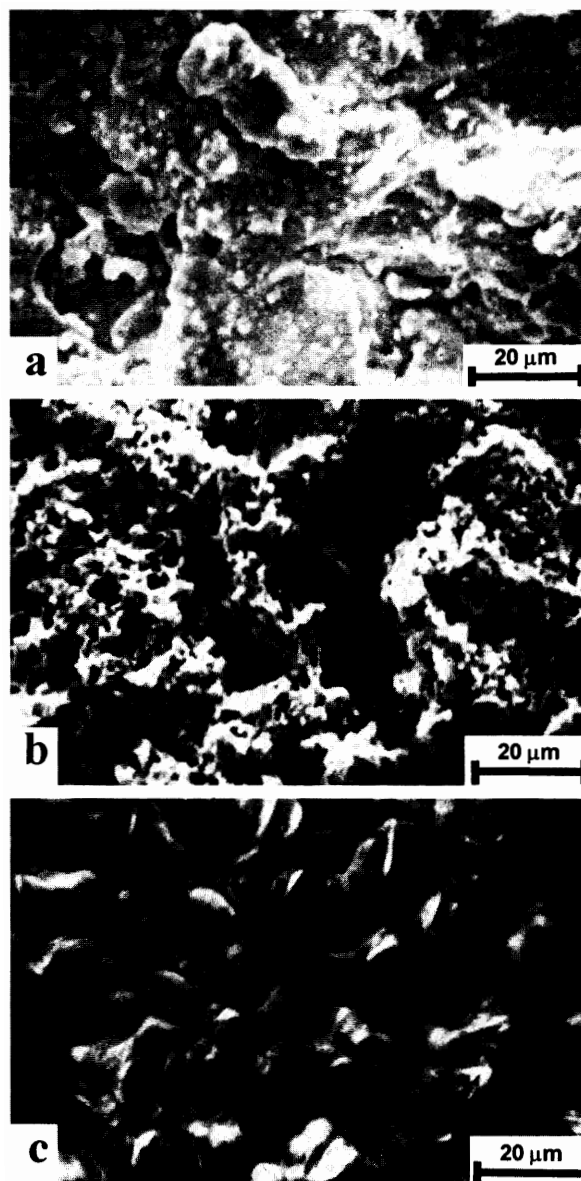


**Fig. 7.** Topography of zirconia specimens: (a) as-sprayed, (b) heat-treated at 873 K for 1.0 h, and (c) heat-treated at 1273 K for 1.0 h.

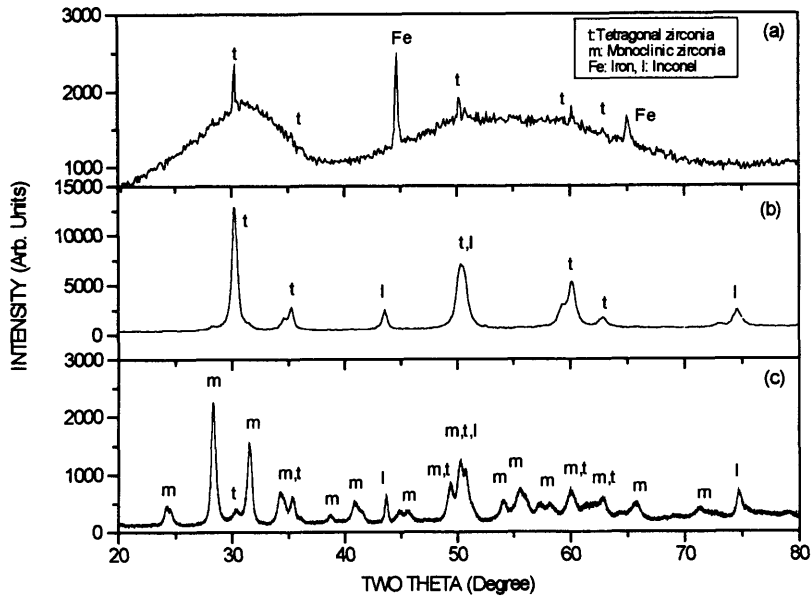


Fig. 8. Variation of XRD of zirconia specimen with heat treatment: (a) as-sprayed, (b) heat-treated at 873 K for 1.0 h, and (c) heat-treated at 1273 K for 1.0 h.



Fig. 9. TEM image of a zirconia specimen heat-treated at 1273 K for 1.0 h.

V. Discussion

Results have shown that the PSLP produces dense hydroxide deposits strongly adherent to the substrates and that the composition and properties of the deposit vary depending on the feedstock, processing conditions, and the heat treatment parameters. In the following sections, the results are discussed based on a simple model.

(1) Modeling of the Deposit Formation

As shown schematically in Fig. 10, by proper design of the atomizer and by varying the atomizer and plasma parameters, aerosol fed deposits can be obtained at four different locations, A, B, C, and D.<sup>11,19,26-29</sup> When there is less heat transfer to the droplets, as when the substrate is placed at location A, incomplete evaporation of the solvent and condensation of the precursor materials occur. This results in liquid droplets splashing on the substrate surface and leads to the formation of a patchy deposit. Chemical reactions occur at or near the substrate surface at location B, leading to an essentially chemical deposition coating, which is dense and adherent. At location C, solid particles have already been formed, but unlike a typical plasma

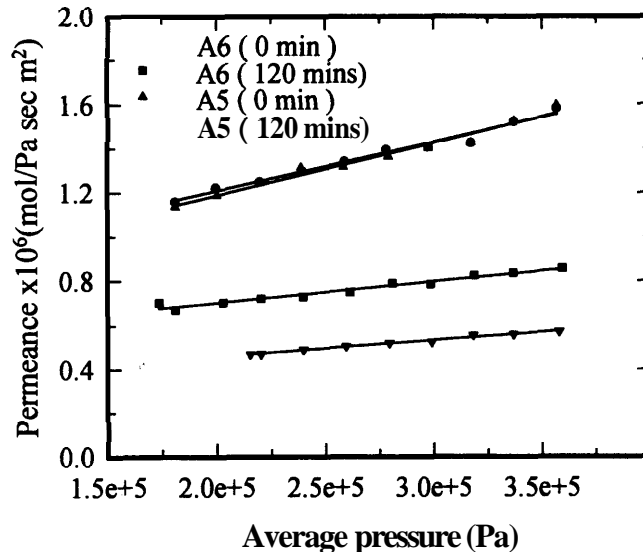


Fig. 10. Schematic of the plasma spray synthesis and deposition process.

spray process, they are not molten. Hence, a powdery deposit is obtained when the substrate is placed at this location. When sufficient heat is transferred by the plasma to the plasma-synthesized particles, they are heated, molten and sprayed onto the substrate, forming a typical thermal spray coating at location D. Thus, high-quality coatings are obtained at positions B and D, while the powder collection is more efficient at location C.

## (2) Atomizer

As noted in Section V(1), the morphology and structure of the sprayed nanodeposit can be varied by controlling the thermal history of the deposited material, and this can be achieved by varying the design and operating parameters of the atomizer to produce different sized droplets. Experiments were performed to produce deposits at the four locations shown in Fig. 10, and they showed the following results:

(a) Efforts to produce a patchy deposit (typically at A) by increasing the liquid feed rate result in nozzle erosion of the plasma torch.

(b) Optimum operation of the atomizer for producing nanosized powder requires the atomizer parameters to be set so that it will produce 1–10  $\mu\text{m}$  sized droplets. However, as-sprayed powdery deposits do not have sufficient adhesive and cohesive strengths, since mechanical keying-in, generated when the molten droplets impinge and spread on the substrate, cannot occur in this case. High-temperature heat treatment is required for enhancing the deposit properties.<sup>12,19,26,29</sup>

(c) Plasma spray beams operate at high jet velocities and pressures.<sup>17</sup> Measurement of the temperature and velocity profiles of droplets injected into the spray jet<sup>22</sup> has shown that the feedstock has a short residence time of only a few milliseconds inside the high-temperature plasma. Hence, even before fully reacted dense particles are formed by nucleation, diffusion, and reactions, they are sprayed away from the hot zone. Thus, these particles cannot be melted by the plasma beam to produce deposits with a lamellar microstructure.

(d) When the atomizer produced aqueous droplets of tens of micrometers in size, the plasma beam could evaporate the water and condense the solid precursor material. The plasma could also drive the decomposition and hydrolysis reactions in the feedstock material at or near the substrate, leading to the formation of chemically deposited layers.

As noted in Section IV(1), the atomizer used in this work produced a wide range of droplet sizes, with a large fraction of them being  $>20 \mu\text{m}$  in diameter. These droplets resulted in the formation of chemically deposited hydroxide deposits, which were strong, dense, and adherent to the substrate.

## (3) Alumina

When aluminum isopropoxide is heated, it is first converted to boehmite and other pseudo-boehmite ( $\text{AlOOH}$ ) phases and then transformed to various alumina phases at different temperatures; i.e.,  $\gamma$  at  $-800 \text{ K}$ ,  $\delta$  at  $-1100 \text{ K}$ ,  $\theta$  at  $-1300 \text{ K}$ , and  $\alpha$  at  $-1400 \text{ K}$ .<sup>30</sup> Though the plasma is at very high temperature, as noted in Section V(1), the residence time of the droplets in the high-temperature zone is only a few milliseconds, and this leads to the formation of the aluminum hydroxide deposit.

The phase transformation from  $\text{AlOOH}$  to  $\gamma$ -alumina is accompanied by about a 35% volume shrinkage, which produces a large number of cracks and pores, requiring densification heat treatment at around  $1273 \text{ K}$ .<sup>30–32</sup> Thus, the as-sprayed coherent and dense pseudo-boehmite deposit converts into a porous  $\gamma$ -alumina coating by low-temperature heat treatment, and the deposit densifies into  $\delta$ -alumina after the high-temperature heat treatment.

The grain sizes of the  $\gamma$ - and  $\delta$ -alumina phases, 7 and 19 nm respectively, compare favorably with the particle/grain size of nano-alumina specimens reported by various authors,<sup>9,32</sup> establishing that EMC plasma spraying of atomized liquid feedstock, followed by heat treatment, is a promising technique for producing nanograined alumina deposits.

## (4) Zirconia

Zirconia is polymorphic with monoclinic, tetragonal, and cubic phases stable at low, medium, and high temperatures, respectively. However, the tetragonal phase is thermodynamically stable even at room temperature, if the crystals are smaller than a critical size.<sup>33,34</sup> When the as-sprayed amorphous  $\text{Zr}(\text{OH})_4$  deposit was heat-treated at low temperature, it produced nanosized grains, and size stabilization resulting in tetragonal zirconia. This result is in agreement with the results of various authors<sup>35–37</sup> who have reported the formation of tetragonal zirconia in nano-zirconia materials. High-temperature heat treatment of highly active nanograins, in general, causes rapid grain growth,<sup>35–37</sup> resulting in the transformation of those grains which have grown larger than the critical size. Thus, the weight fraction of tetragonal zirconia present in nanosized zirconia varies with the thermal history of the specimen and its initial microstructure.<sup>35–37</sup> Hence, the formation of monoclinic zirconia as the predominant phase in the high-temperature heat-treated specimen shows that considerable grain coarsening has occurred during the densification treatment. The results of the Scherrer analysis confirm this observation, showing that the grain size increases by an order of magnitude.

The grain sizes of the zirconia deposits compare well with the particle/grain sizes of nano-zirconia specimens prepared by different techniques,<sup>35–37</sup> confirming the feasibility of producing plasma-sprayed nano-zirconia deposits.

## VI. Conclusions

Nanostructured deposits have been prepared by plasma spraying of liquid precursor feedstocks. The results of this study can be summarized as follows.

(1) Nanodeposits can be produced by injecting atomized liquid droplets of precursor solution into the EMC plasma flame.

(2) Plasma spraying of aqueous feedstock solutions leads to the formation of dense and adherent hydroxide deposits. Postspray calcination at  $873 \text{ K}$ , followed by high-temperature heat treatment at  $1273 \text{ K}$ , produces dense and strong oxide deposits with nanosized grains.

(3) Spray, feedstock, and heat treatment parameters strongly influence the grain size, microstructure, and phase composition of the nanodeposits.

**Acknowledgments:** We would like to thank Prof. J. R. T. Branco of the Metallurgical Technology Department, Minas Gerais Technology Center Foundation—CETEC, Minas Gerais, Brazil, for many stimulating discussions, and K. A. Kowalsky and D. R. Marantz of Flame Spray Industries, Stony Brook, and Dr. J. Quinn of the Department of Materials Science and Engineering for experimental assistance.

## References

- <sup>1</sup>H. Gleiter, "Nanocrystalline Materials," *Prog. Mater. Sci.*, **33**, 223–315 (1990).
- <sup>2</sup>C. C. Koch, "The Synthesis and Structure of Nanocrystalline Materials Produced by Mechanical Attrition: A Review," *Nanostruct. Mater.*, **2**, 109–29 (1993).
- <sup>3</sup>B. H. Kear, L. E. Keem, R. W. Siegel, F. Spaepen, K. C. Taylor, E. L. Thomas, and K. N. Tu, "Research Opportunities for Materials with Ultrafine Microstructures," Vol. NMAB-454, National Academy, Washington, DC, 1989.
- <sup>4</sup>M. Gell, "Applying Nanostructured Materials to Future Gas Turbine Engines," *J. Met.*, [Oct.] 30–34 (1994).
- <sup>5</sup>R. W. Siegel, "Nanostructured Materials—Mind over Matter," *Nanostruct. Mater.*, **3**, 1–18 (1993).
- <sup>6</sup>R. Uyeda, "Studies of Ultrafine Particles in Japan: Crystallography, Methods of Preparation and Technological Application," *Prog. Mater. Sci.*, **35**, 1–96 (1991).
- <sup>7</sup>H. Gleiter, "Materials with Ultrafine Microstructures; Retrospectives and Perspectives," *Nanostruct. Mater.*, **1**, 1–20 (1992).
- <sup>8</sup>C. J. Brinker and G. W. Scherer, *Sol-Gel Science: The Physics and Chemistry of Sol-Gel Processing*, Academic Press, San Diego, CA, 1990.
- <sup>9</sup>B. Gunther and A. Kumpmann, "Ultrafine Oxide Powders Prepared by Inert Gas Evaporation," *Nanostruct. Mater.*, **1**, 27–30 (1992).
- <sup>10</sup>G. F. Gaertner and P. F. Miquel, "Particle Generation by Laser Ablation from Solid Targets in Gas Flows," *Nanostruct. Mater.*, **4**, 559–68 (1993).
- <sup>11</sup>J. L. Katz and P. F. Miquel, "Synthesis and Applications of Oxides and

Mixed Oxides Produced by a Flame Process," *Nanostruct. Mater.*, 4, 551–57 (1994).

<sup>12</sup>Y. Mizoguchi, M. Kagawa, M. Suzuki, Y. Syono, and T. Hirai, "Synthesis of Ultrafine Particles and Thin Films of BaFe<sub>12</sub>O<sub>19</sub> by Spray ICP Technique," *Nanostruct. Mater.*, 4, 541–96 (1993).

<sup>13</sup>D. Vollath and K. E. Sickafus, "Synthesis of Nanosized Ceramic Oxide Powders by Microwave Plasma Reactions," *Nanostruct. Mater.*, 1, 427–37 (1992).

<sup>14</sup>R. J. Dowling, J. J. Stiglich, and T. S. Sudarshan, "Synthesis and Consolidation of Nanoparticles"; pp. 45–58 in *Specialty Materials and Composites*. Edited by C. Lall and A. J. Neupaver. Metal Powder Industries Federation, APMI International, Princeton, NJ, 1994.

<sup>15</sup>M. Kagawa, Y. Imamura, S. Usui, and Y. Syono, "Distribution of ZrO<sub>2</sub> and Al<sub>2</sub>O<sub>3</sub> in Ultrafine ZrO<sub>2</sub>-Al<sub>2</sub>O<sub>3</sub> Powders Formed by the Spray-ICP Technique," *J. Mater. Sci. Lett.*, 3, 699–702 (1984).

<sup>16</sup>L. Powlowski, *The Science and Engineering of Thermal Spray Coatings*. Wiley, New York, 1995.

<sup>17</sup>C. Brunet and S. Dallaire, "The Importance of Particle Size Distribution on the Plasma Spraying of TiC," *Surf Coat. Technol.*, 31, 1–10 (1987).

<sup>18</sup>R. A. Neiser, "Structure-Processing-Property Relationships in Air Plasma Sprayed Y<sub>1</sub>Ba<sub>2</sub>Cu<sub>3</sub>O<sub>7-8</sub>"; Ph.D. Thesis. State University of New York, Stony Brook, NY, 1989.

<sup>19</sup>A. Gurav, T. Kudas, T. Pluym, and Y. Xiong, "Aerosol Processing of Materials," *Aerosol Sci. Technol.*, 19, 411–52 (1993).

<sup>20</sup>D. R. Marantz, "Electromagnetically Coalesced Multi-Arc Plasma Torch with True Axial Powder Feed"; pp. 443–50 in *Thermal Spray Research and Applications*. Edited by T. F. Bernecki. ASM International, Materials Park, OH, 1991.

<sup>21</sup>R. H. Perry, *Perry's Chemical Engineers' Handbook*, 6th ed. McGraw-Hill, New York, 1984.

<sup>22</sup>J. Tikkanen, J. Karthikeyan, V. Pitkanen, J. Keskinen, K. A. Gross, S. Raghu, M. Rajala, and C. C. Berndt, "Characterization of the Liquid Flame Spray Process," submitted to *Surf Coat. Technol.*

<sup>23</sup>H. P. Klug and L. E. Alexander, *X-ray Diffraction Procedure for Polycrystalline and Amorphous Materials*, 2nd ed. Wiley, New York, 1974.

<sup>24</sup>T. Ekstrom, C. Chatfield, W. Wruss, and M. M. Schreiber, "The Use of X-ray Diffraction Peak Broadening to Characterize Ground Al<sub>2</sub>O<sub>3</sub> Powders," *J. Mater. Sci.*, 20, 1266–74 (1985).

<sup>25</sup>S. K. Pradhan, T. Chakraborty, S. P. Sen Gupta, C. Suryanarayana, A. Frefer, and F. H. Froes, "X-ray Powder Profile Analysis on Nanostructured Niobium Metal Powders," *Nanostruct. Mater.*, 5, 53–61 (1995).

<sup>26</sup>C. Roger, T. Corbitt, C. Xu, D. Zeng, Q. Powell, M. Nyman, M. J. Hampden-Smith, and T. T. Kudas, "Principles of Molecular Precursor Selection for Aerosol Synthesis of Materials," *Nanostruct. Mater.*, 4, 529–35 (1994).

<sup>27</sup>I. Wiedemann, K. L. Choy, and B. Derby, "Flame-Assisted Deposition of Lead Titanate-Based Thin Films; Correlation of Deposition Process, Microstructure and Electrical Properties"; 133–142 in *Novel Synthesis and Processing of Ceramics*. Edited by F. R. Sale. The Institute of Materials, London, U.K., 1994.

<sup>28</sup>S. K. Freilander, R. S. Windeler, and A. P. Weber, "Ultrafine Particles Formation in Turbulent Jets: Mechanisms and Scale-up," *Nanostruct. Mater.*, 4, 521–28 (1994).

<sup>29</sup>J. Karthikeyan, C. C. Berndt, J. Tikkanen, S. Reddy, and H. Herman, "Spray Synthesis of Nanomaterial Powders and Deposits," unpublished work.

<sup>30</sup>W. H. Gitzen (Ed.), *Alumina as a Ceramic Material*. American Ceramic Society, Columbus, OH, 1970.

<sup>31</sup>L. C. Klein, "Oxide Coatings from the Sol-Gel Process," *Ceram. Eng. Sci. Proc.*, 5, 379–84 (1984).

<sup>32</sup>C. M. Wang and F. L. Riley, "Morphological Changes During the Calcination of Oxide-Coated Silicon Nitride Powder"; pp. 235–48 in *Novel Synthesis and Processing of Ceramics*. Edited by F. R. Sale. The Institute of Materials, London, U.K., 1994.

<sup>33</sup>R. C. Garvie and M. V. Swain, "Thermodynamic Analysis of the Tetragonal to Monoclinic Transformation in a Constrained Zirconia Microcrystal, Part I," *J. Mater. Sci.*, 20, 1193–200 (1985).

<sup>34</sup>C. A. Anderson and P. K. Gupta, "Phase Stability and Transformation Toughening in Zirconia"; pp. 184–201 in *Advances in Ceramics*, Vol. 3, *Science and Technology of Zirconia*. Edited by A. H. Heuer and L. W. Hobbs. American Ceramic Society, Columbus, OH, 1981.

<sup>35</sup>D. J. Chen and M. J. Mayo, "Densification and Grain Growth of Ultrafine 3 mol% Y<sub>2</sub>O<sub>3</sub>-ZrO<sub>2</sub> Ceramics," *Nanostruct. Mater.*, 2, 469–78 (1993).

<sup>36</sup>G. Skandan, "Processing of Nanostructured Zirconia Ceramics," *Nanostruct. Mater.*, 5, 111–26 (1995).

<sup>37</sup>V. V. Lapatin, U. F. Ivanov, and V. S. Dedkov, "Structure-Diffraction Analysis of Nanometer-Sized Polycrystals," *Nanostruct. Mater.*, 4, 669–76 (1994). □